through spin polarization of an sp^2 orbital. It is not appropriate for proton interaction through spin polarization of its 1s orbital unless if multiplied by the factor[20] $3\times507.6/1191$. This slightly modifies Colpa and de Boer's second-order term to $+0.83$ and the resulting theoretical value is $Q_{C'C}{}^H=-0.9$ G.

Colpa and de Boer make several serious approximations in their calculation and in addition their calculation does not exactly apply to our case. Their calculation is for sp^2 hybridization with the H atom in the usual pi-electron nodal plane, while our determination is for sp^3 hybridization with the H atoms in a nodal plane between two pi orbitals. The first-order contribution can be quite different in the two cases for the exchange integrals between the pi-electron and the C–H orbitals are dependent upon the angle between them. It is quite possible, however, that the McLachlan calculation given in Table I contains most of the correction for the C–H bond not being in the usual pi-electron nodal plane. If this is the case, then the agreement between Morton's value and our positive value of $Q_{C'CH}{}^H$ is good evidence that the Colpa and de Boer calculation gives the wrong sign for spin polarization.

ACKNOWLEDGMENTS

We are indebted to Professor F. R. Jensen for supplying our first sample of cycloheptatriene and for help with the deuteration. Miss Carolyn Talcott prepared the deuterated species and did some of the computer calculations. This work was supported by a grant from the U.S. Atomic Energy Commission.

THE JOURNAL OF CHEMICAL PHYSICS VOLUME 43, NUMBER 9 1 NOVEMBER 1965

Spin–Orbit Coupling and Electron-Affinity Determinations from Radiative Capture of Electrons by Oxygen Atoms

R. STEPHEN BERRY* AND JOHN C. MACKIE

Department of Chemistry and Institute for the Study of Metals, University of Chicago, Chicago, Illinois

AND

RAYMOND L. TAYLOR AND ROBERT LYNCH†

Avco-Everett Research Laboratory, Everett, Massachusetts

(Received 27 April 1965)

The radiative capture continuum for the process $O^0+e\rightarrow O^-+h\nu$ is studied in the region of the threshold, 7800–8800 Å. The spectrum is produced in shock-heated vapors of potassium peroxide and rubidium oxide in neon and argon. Individual thresolds are resolved which correspond to the transitions $O(^3P_2)\rightarrow O^-(^2P_{\frac{3}{2}})$, $O(^3P_2)\rightarrow O^-(^2P_{\frac{1}{2}})$, $O(^3P_1)\rightarrow O^-(^2P_{\frac{1}{2}})$, and possibly $O(^3P_0)\rightarrow O^-(^2P_{\frac{1}{2}})$. From these thresholds, the electron affinity of the oxygen atom is determined to be 1.478 ± 0.002 eV and the separation of $^2P_{\frac{1}{2}}$, $^2P_{\frac{3}{2}}$ states of O^-, 285 ± 15 cm^{-1}, corresponding to a spin–orbit coupling constant of 190 ± 10 cm^{-1} for the oxygen negative atomic ion.

I. INTRODUCTION

DIRECT capture of a free electron by a neutral atom leads to the emission of radiation and the formation of a negative atomic ion, according to Process (1):

$$O^0+e^-\rightarrow O^-+h\nu. \qquad (1)$$

The spectrum of the emitted radiation is continuous above a threshold frequency ν_0. We report here a study of this process, the radiative capture of electrons, in the case of capture by free gaseous oxygen atoms. Our concern here lies entirely with the region of the spectrum within about 1000 cm^{-1} of the threshold and the information to be derived from this part of the capture spectrum. The principal results of our investigation are values for the electron affinity of the oxygen atom and especially of the spin–orbit coupling constant of the atomic oxygen negative ion O^-.

The region in which the threshold lies is already well known. Branscomb, Burch, Smith, and Geltman studied the process (2) of photodetachment of electrons from free atomic negative ions of oxygen[1]:

$$O^-+h\nu\rightarrow O^0+e^-. \qquad (2)$$

They were able to determine a frequency for the threshold and a value of the electron affinity of the oxygen

* Alfred P. Sloan Fellow.

† Present address: Department of Physics, Brandeis University, Waltham, Massachusetts.

[1] L. M. Branscomb, D. S. Burch, S. J. Smith, and S. Geltman, Phys. Rev. **111**, 504 (1958).

atom of 1.465±0.005 eV. This value is consistent with the dissociative attachment of electrons to oxygen molecules as interpreted by Chantry and Schulz[2]; dissociative attachment, analyzed in terms of its dependence on electron and O^- ion energies, leads to a value of 1.5±0.1 eV for the electron affinity of oxygen. We expected, therefore, to find a threshold for continuous emission at 8460±30 Å for the radiative capture process (1).

The reason for choosing radiative capture, (1), rather than photodetachment, (2), becomes clear shortly. Radiative capture of electrons by oxygen has been reported previously, by Boldt.[3] He analyzed the total emission from a wall-stabilized arc in the region 4300–6300 Å, and concluded that, under his conditions, a significant fraction of the emitted radiation was due to Process (1). Unfortunately Boldt's wavelength span did not extend far enough to include the threshold region.

In the present work, we have studied the capture process (1) spectroscopically, under moderately high resolution. Our objectives in this work were twofold. Firstly we intended to determine conclusively whether the high-temperature spectroscopic method yields electron affinities identical with those obtained by the crossed-beam photodetachment method.[1,4] Secondly, we have sought to resolve the spectrum in the threshold region into its component thresholds arising from the three states of the $O^0(^3P)$ term and the two states of $O^-(^2P)$.

Since the crossed-beam method utilizes a low-density stream of mass-analyzed negative ions, no ambiguity occurs in the identification of the ion and no problem of possible effects of the medium arises. The spectroscopic method used to study the photodetachment spectra of the halide ions and electron affinities of the halides[5,6] can, in principle, suffer from both these deficiencies. (In the case of the halides neither effect was a problem.) Only one ion, the iodide ion, has been studied by both methods[5,7]; in that case the two approaches give essentially identical values for the electron affinity of the iodine atom. We nevertheless felt that a firmer confirmation of the validity of the spectroscopic method would be in order, and that the O^- ion would provide an appropriate test.

Validation of the high-temperature spectroscopic method is particularly important because of the high spectral resolution that it offers. This resolution has already been used to study the shape of halide-ion photodetachment cross sections near their thresholds and the effect of ionic media on these shapes.[8] Our intent in attaining high resolution in the study of the O^- ion via the emission from Process (1) was: (a) identifying the emission continuum by observing threshold separations equal to the known spacings of the $^3P_0$, $^3P_1$, and $^3P_2$ states of the oxygen atom, and (b) determining the spin–orbit coupling constant of O^- by measuring the threshold separations corresponding to the $^2P_{\frac{3}{2}}$ and $^2P_{\frac{1}{2}}$ states of O^-. This would be the first negative ion for which the spin–orbit coupling has been measured.

II. DISCUSSION OF METHOD

The spectroscopic observation of O^- can, in principle, be carried out equally well as an absorption problem according to (2) or as an emission problem, (1). The emission method for observing thresholds was demonstrated sucessfully for the halogens.[9,10] The halogen radiative capture thresholds[9] all coincided with the photodetachment thresholds observed in absorption, so that there seemed to be no anomalies arising from the somewhat different conditions required for the two processes.

The basic approach for the spectroscopic method is simply to prepare a system in which the species one wishes to study are present at equilibrium in suitably high concentration. For absorption, this means preparing a sizeable concentration of the negative ion. For radiative capture, one needs a large concentration of electrons and of the atoms in question.

We now examine the intensity of emission from Process (1) and its frequency dependence. In so doing, we may make a general inference of the ranges of conditions in which Processes (1) and (2) are each useful for studying negative-ion properties. The most convenient starting point is the Beer's law expression for Process (2) in terms of the photodetachment cross section $\sigma_{\text{det}}(\nu)$, the incident and transmitted intensities $I_0(\nu)$ and $I(\nu)$, the path length l(centimeters) and $n(O^-)$, the concentration of absorbers, O^- ions per cubic centimeter:

$$\ln[I_0(\nu)/I(\nu)]=\sigma_{\text{det}}(\nu)n(O^-)l. \qquad (3)$$

The photodetachment cross section for O^- near its threshold[4,11] is about 10^{-18} cm^2. A typical concentration of O^- in a very favorable environment, for example a vapor of cesium oxide at 4000°K and containing 10^{16} dissociated CsO molecules per cubic centimeter, is only 2.3×10^{12} cm^3. The light path l required to make I_0/I

[2] P. J. Chantry and G. J. Schulz, Phys. Rev. Letters **12,** 449 (1964).
[3] G. Boldt, Z. Physik **154,** 319 (1959).
[4] L. M. Branscomb, in *Atomic and Molecular Processes*, edited by D. R. Bates (Academic Press Inc., New York, 1962), Chap. 4, pp. 100ff.
[5] R. S. Berry, C. W. Reimann, and G. N. Spokes, J. Chem. Phys. **37,** 2278 (1962).
[6] R. S. Berry and C. W. Reimann, J. Chem. Phys. **38,** 1540 (1963).
[7] B. Steiner, M. L. Seman, and L. M. Branscomb, in *Atomic Collision Processes*, edited by M. R. C. McDowell (John Wiley & Sons, Inc., New York, 1963), p. 537.
[8] R. S. Berry, C. W. David, and J. C. Mackie, J. Chem. Phys. **42,** 1541 (1965).
[9] R. S. Berry and C. W. David, Ref. 7, p. 543.
[10] H. Henning, Z. Physik **169,** 467 (1962).
[11] S. J. Smith, Proc. Intern. Conf. Ionization Phenomena Gases, 4th Uppsala 1959, 219 (1960).

significantly different from unity in this case is about 10^6 cm. This is a rather impractical length for a system at the required temperature.

Clearly the feasibility of any absorption experiment hangs on the magnitude of the negative-ion concentration that can be attained in the laboratory. Provided a good electron source like an alkali is present, the maximum value of the negative-ion concentration, $n_{\max}(X^-)$ is determined in the main by the Boltzmann factor $\exp(E.A./kt)$. As we just saw, if the electron affinity (E.A.) is about 1.5 eV, $n_{\max}(X^-)$ can only reach 10^{12}cm^{-3}, too low by two orders of magnitude for absorption spectroscopy. However, if the affinity of X is 2 eV or more, then the concentration of X^- can reach 10^{14} cm^{-3} or more. In effect, 2 eV represents a sort of practical limiting value of the electron affinity for spectroscopic purposes. If E.A.(X) is greater than 2 eV, then X^- can probably be observed in conventional absorption spectroscopy; if E.A.(X) is less than 2 eV, conditions for studying X^- in absorption cannot be reached with present techniques.

For low-affinity species, radiative attachment (1) is the more natural method of observation. The attachment cross section σ_{att} is related to the corresponding detachment cross section by the condition of microscopic reversibility:

$$\sigma_{det}/g(O^-)m_e^2v_e^2=\sigma_{att}c^2/g(O^0)h^2\nu^2, \qquad (4)$$

where $g(x)$ is the degeneracy of Species x, and m_e, v_e are the mass and velocity of the electron. The relevant observable for emission is not log$I$ but I itself. The rate of emission of quanta of energy $h\nu$, per unit of frequency, is

$$I(\nu)/h\nu=\dot{N}(\nu)$$
$$=\sigma_{att}(\nu)v_e(\nu)n(e)n(O^-)\rho_e. \qquad (5)$$

We let ρ_e be the energy distribution function for the electrons and neglect the atomic velocities compared with v_e. From (4) and the absolute photodetachment cross section measured by Smith,[11] we find that the radiative attachment coefficient

$$\alpha_{att}(\nu)=\sigma_{att}(\nu)v_e(\nu) \qquad (6)$$

is approximately 10^{-15} cm^3/sec near threshold. The energy distribution function, expressed explicitly in terms of electron velocity and in units of wavenumbers^{-1}, is

$$\rho_e=(2m/\pi k^3T^3)^{\frac{1}{2}}hv_e\exp(-m_ev_e^2/2kT). \qquad (7)$$

Then with a typical set of concentrations of electrons and oxygen atoms, say 10^{16} cm^{-3} of each, and with a temperature of about 4000°K, we can expect to find about 10^{11} quanta emitted per cubic centimeter per second per wavenumber of bandwidth near threshold.

Even more important, we find, from the threshold behavior of $\sigma_{det}(\propto v_e)$ and from (7), that the emitted intensity given by (5) shows a sharp threshold:

$$I\propto v_e \quad \text{or} \quad (\nu-\nu_0)^{\frac{1}{2}}. \qquad (8)$$

Anticipating further discussion, we can point out that the actual emission spectra described here were taken with time-resolving drum-camera spectrographs set to observe the light emitted from alkali oxides which were vaporized and dissociated by means of a shock wave. The useful observation time is about 50 μsec, and the useful observation volume is roughly 10 cm^3, from which at least 10^{-4} of the total solid angle is actually collected into the spectrograph. From these figures, we estimate that about 10^4 quanta strike a slit image on the film. This is a relatively easy number to record. From the figures and from Expression (8), we therefore expect the emission spectrum to be observable and to exhibit the characteristic $(\nu-\nu_0)^{\frac{1}{2}}$ dependence.

The actual concentrations of electrons and oxygen atoms that one can expect to obtain can be calculated readily from spectroscopic data.[12] Figure 1 shows a typical set of such concentrations, for vaporized potassium peroxide K_2O_2. The only molecule expected to be present in high concentration is the diatomic KO, and its concentration clearly drops rapidly with increasing temperature. No allowance for ionization of oxygen atoms was made in the calculation, but under the actual conditions, such as those shown in the graph, the inclusion of O^+ does not affect the neutral-oxygen concentration detectably. From the figure, it is easy to see that temperatures above 4000°K are very desirable. We consequently chose to use reflected shock conditions for observing the radiative attachment process.

It is abundantly clear from calculations like those used for Fig. 1 that a good electron source, something much better than oxygen itself, is of vast assistance to Reaction (1). For this reason we followed the idea generated in earlier work on halide ions and used alkali oxides as the source of oxygen atoms and electrons. If oxygen itself were the source of both species, the temperature would have to be at least 10 000°K and preferably somewhat higher for the capture process to be detectable. The range 10 500°–13 000°K was actually typical in Boldt's work. Temperatures as high as these present the problem that emission from free–free transitions is rather intense, enough to become a serious problem when the emission spectra are analyzed in terms of the various contributing processes. When the electron source is an alkali like rubidium or potassium,

[12] From the calculations of L. Brewer and D. F. Mastick, [J. Am. Chem. Soc. **73**, 2045 (1951)], it is clear that at the temperatures of interest, the only molecule expected to be present in appreciable concentration is the diatomic KO. Following the procedure of E. S. Ritter [J. Chem. Phys. **19**, 1030 (1951)] we can calculate the dissociation energy of KO, the vibrational frequency, and the rotational constant by assuming an ionic model. The equilibrium concentrations of the species present in the vapor can be computed from a knowledge of the foregoing quantities together with the energy levels and ionization potential of the alkali and the electron affinity of oxygen.

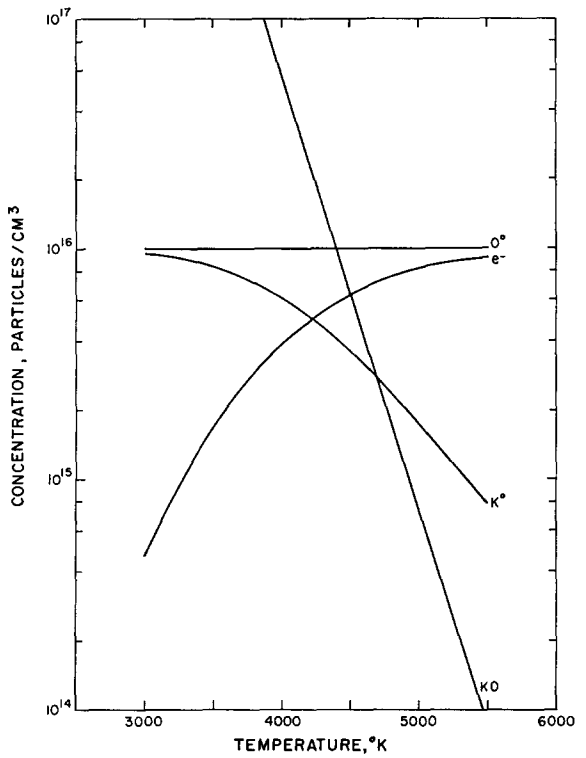

FIG. 1. Calculated concentrations of oxygen atoms, electrons, potassium atoms, and KO molecules at equilibrium thermodynamic conditions, as functions of temperature, if the concentration of dissociated KO is 10^{16} cm^{-3}. A first-order correction was made for the activity of the ions due to ion–ion interactions; this amounted to only a few percent of the concentration.

the required temperatures are low enough that Bremsstrahlung is not a serious interference and can in fact be eliminated virtually completely.

III. EXPERIMENTAL

A. Apparatus

The apparatus consisted basically of a mechanically (gas.)driven shock tube equipped with observation windows near the end plate and a rotating-drum spectrograph of high aperture and medium dispersion capable of recording near-infrared spectra. Two completely separate units were used. A stainless-steel tube, whose test section had a $1\frac{1}{2}$-in.-square cross section, was used for most of the exploratory work and for confirmatory data. Two time-resolving instruments were used with this tube, a streak camera recording total visible light on an x–t photograph and a small rotating-drum spectrograph. The final experiments, from which were taken the bulk of the measurements and data reported here, were made with a mild-steel tube equipped with a stainless-steel test section. (Spectra of reflected shocks in a mild-steel tube consisted of many iron lines which obscured all other features.) This tube has a $3\frac{1}{2}$-in.-square internal cross section. The drum camera used for this work utilizes a plane-grating spectrograph designed by C. David. Its aperture is $f/4$ and, with a 600-line/mm Bausch & Lomb diffraction grating, gives a dispersion of approximately 28 Å/mm across a strip of 35-mm film. The actual resolution is at least eight times that required to resolve the smallest splitting, 68 cm^{-1}, due to fine structure in the neutral O atom. The drum speed was varied to give time dispersions between 3 and 10 μsec/mm, and the slit height was usually 1 mm. Drum speeds could be measured with a tachometer. The spectral slitwidths ranged from 20 to 50 μ, corresponding to 0.6 to 1.5 Å or 1.5–2.5 cm^{-1} at the focal plane.

B. Sample Introduction and the Vaporization Process

The sizes of sample were varied between 0.2 and 1 g. Samples larger than 600 mg were not completely vaporized; samples smaller than about 400 mg gave continua that were rather weak for good microdensitometry. Between these limits, the sample size was not at all critical.

The alkali oxide samples were placed on supporting material of either aluminum foil or cleansing tissue and the support was taped across the tube. The sample must be in a position so that some of the vaporized oxide passes in front of the window. If the sample were initially too far upstream, the reflected shock could in principle keep the sample from reaching the window; on the other hand, if it were too far downstream, the sample might not have time to evaporate.

Previous considerations indicated that the optimum position can be calculated from the assumption that the initial position of the salt becomes the position of a stationary source of salt vapor in laboratory coordinates. The flowing carrier gas carries off vapor as it evaporates the shocked particles of alkali oxide.

The mechanism of salt vaporization has been studied in two ways:

(1) We have varied the position, upstream and downstream, from the optimal point determined by the model. These spanned the entire range from "too far upstream" to "too far downstream." Between was a range of several inches over which there was no significant change in the continuous radiation from the reflected shocked gas containing alkali oxide. We obtained flexibility by varying the position of observation window and sample. This variation can be used to achieve either of two conditions; the reflected shock may reach the window either before or after the salt itself reaches the window. The "material front," the surface defining the farthest downstream penetration of salt vapor, travels at the particle velocity in the shocked gas. This velocity is of course less than the velocity of either incident or reflected shock. Hence the reflected shock returns up the tube to meet the material front and may reach it before the material front passes the point of observation or afterwards. If the meeting occurs after-

wards, as it did in many of our later experiments, there is no problem in observing the salt provided it has already vaporized. If the meeting occurs before the material front passes the window, it seems possible that no emission from the salt would be observed, simply because the salt behind the material front might be stopped at the point of intersection of the material and reflected shock fronts, or at least severely retarded there. In fact, this retardation is not severe; the high-density gas containing salt vapor is transmitted effectively into the low-density gas of the reflected shock.

(2) We took x–t records of the total visible light in the region between the end wall and a point 5.2 cm away. The spectrograph was set to observe a point approximately 3 cm from the end wall. A typical x–t record and the corresponding t–λ record are shown in Fig. 2.

In the original photograph, the incident shock (indicated by the dashed line in Fig. 2) is almost invisible because of its low luminosity. The reflected shock is clearly apparent, and the very high luminosity following the reflected shock is due to the alkali oxide entering the reflected shock zone. At the time the luminosity due to salt reaches the spectrographic point of observation, the emission changes from a line spectrum of argon, in this case, to a mixture of alkali lines and continuum. The latter is due mostly, as we demonstrate, to radiative capture of electrons by oxygen atoms.

C. Data Collection and Analysis

Spectra were taken of shocks containing K_2O_2, Rb_2O, and a number of control substances. These included pure inert carrier gases (Ne and Ar), supporting materials alone (Al foil and cleansing tissue), and alkali halides. The spectra were recorded under different shock conditions and at different angular settings of the grating, to eliminate artifacts of the apparatus. A filter served to eliminate higher orders of dispersion. The optimum shock conditions corresponded roughly to driving pressures of 550–700 psi of hydrogen and 4.0–7.0 cm Hg of argon or 2.5–5.0 cm Hg of neon. The shocks made with neon carrier were much freer of continuous background radiation, to the extent that the correction for this radiation was negligible in the wavelength region 8100–8600 Å.

Small variations of the grating orientation showed that our optical system produces a slightly nonuniform illumination of the focal plane, so that wavelengths at the high-energy side of the film receive more light than those on the low-energy side. This effect was taken into full account very easily both by calibration and by the variation of grating orientation.

Films were developed for 4 min in D-19 developer at 68°±2°C. The dried films were either taped to glass plates or mounted between glass plates and measured with a Jarrell-Ash Model 24-300 recording microdensitometer. Some care was required to avoid Newton's rings. Calibrations were made with a Jarrell-Ash seven-step neutral density filter and a tungsten lamp.

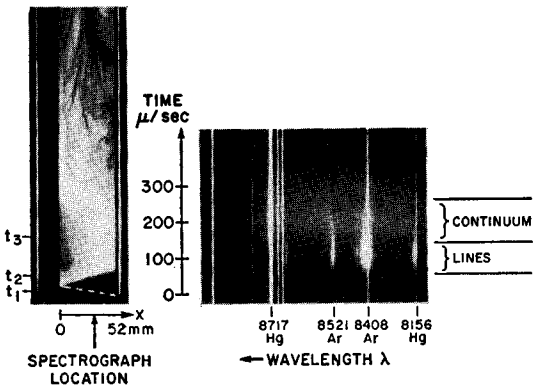

FIG. 2. A typical x–t photograph (left), and the corresponding λ–t time-resolved spectrum (right) of Rb_2O on Al. The two photographs are shown here with the same time (vertical) scale, with time increasing upward. The left-hand photograph exhibits the entire visible light emitted from a horizontal slit parallel to the axis of the shock tube (x axis) as a function of time. As indicated, the slit extended from the end wall of the shock tube to a point 5.2 cm upstream. The almost nonluminous incident shock, which is only barely visible on the original photograph, is indicated by the dashed diagonal line from lower right toward upper left. At the rear wall ($x=0$), the reflected shock returns, highly luminous, and shows as an intense band moving upward toward the right. The material front then penetrates the reflected shock and becomes extremely bright as it moves toward $x=0$. The spectrograph x position is indicated. On the left of the x–t photograph are the times t_1, t_2, and t_3. At t_1, the incident shock passes the spectrograph; at t_2, the reflected shock passes the spectrograph, and the spectrum (right photograph) develops a number of lines, principally of the carrier gas (argon in this instance). At t_3, the material front crosses the slit, and the luminosity changes from line to line, band, and continuum emissions. New lines, e.g., Rb in this case, appear at t_3, and in some cases, diatomic bands as well. The O^- continuum always appears at t_3. At approximately 250 μsec, rarefaction waves appear which cool the gas and end the experiment. $P_1=5.0$ cm Hg of Ar; $U_s=2.60$ mm·μsec.

Identifiable atomic lines acted as internal standards for measuring wavelengths. Direct measurement on the microdensitometer records proved to be entirely sufficient for this purpose. Of the spectral lines observed almost all were identified. Impurity and metal lines included: 8662, 8542, and 8498 Å, Ca^+; 8521, Cs^0; 8195, 8183, Na^0; 8271, 7948, 7800, Rb^0; 8629, 8594, 8568, 8242, 8223, 8216, 8210, 8188, N^0. Molecular bands observed in absorption were: 8652, 8153, CaO; 8634, 8566, 8375, 8309, 8266, K_2. The 8448 line of oxygen, the 8654 line of Ne, and the argon lines at 8521, 8424, 8404, 8264, 8115, and 8104 Å were also readily observed. A number of weak bands of K_2 and Rb_2 were observed in absorption but not measured.

Figure 3(a) is a typical spectrum taken with 28-Å/mm wavelength dispersion, a time scale of 10 μsec/mm, and a slit height of approximately 1 mm. With the spectrum is a pair of typical microdensitometer traces [Fig. 3(b)]; the upper trace is taken from the displayed spectrum, and the other from a slightly less intense spectrum taken under slightly different conditions. The

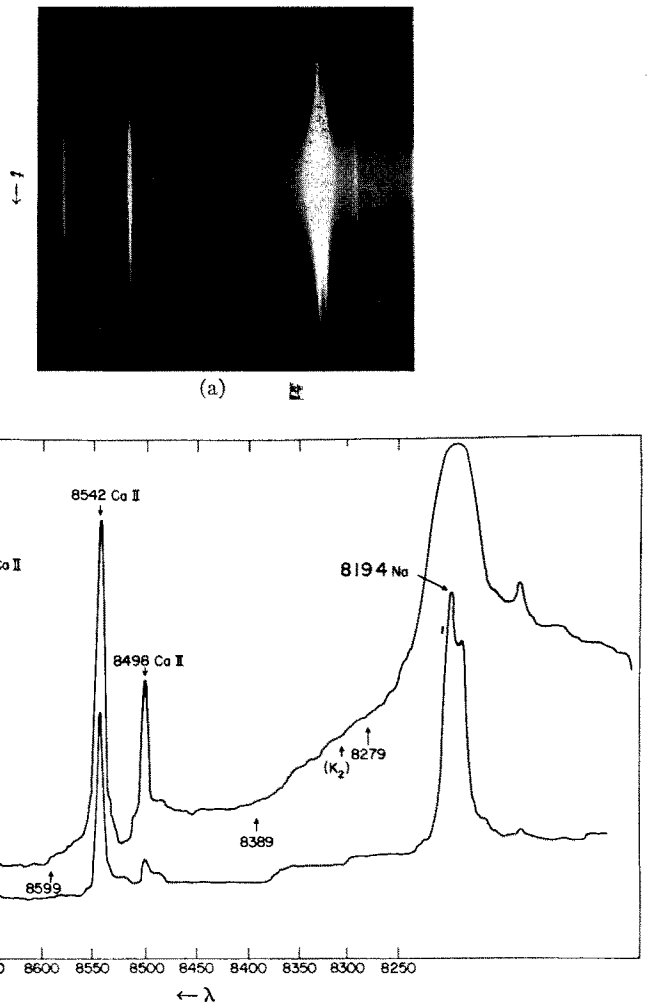

FIG. 3. A typical time-resolved spectrum taken under 28-Å/mm dispersion (a), together with two typical microdensitometer tracings (b). The spectrum is that of shock-heated K_2O_2 in neon. The upper tracing was taken from the spectrum above, and the lower, from a somewhat less intense spectrum.

microdensitometer traces were made with approximately the same slit height as that used in the spectrograph.

The tracings shown in Fig. 3 are typical. The intensity fluctuations in the upper curve between 8390 and 8250 Å are not noise; they are clearly identifiable on the film and have been assigned. Most are due to K_2—one of the strongest of these is indicated in the figure. The fluctuations at 8279 and 8599 are not assignable to K_2.

The spectra and uncorrected traces clearly show marked rises in intensity in the regions near 8590, 8390, and 8275 Å. The region from about 8520 to 8460 is obscured by lines of the ubiquitous Ca^+, and the shoulder of the Na resonance line at 8195 makes it very difficult to distinguish weak features at wavelengths as short as 8240 or 8250. Aside from these two interferences, the spectral region where the radiative capture thresholds are expected is rather clear, particularly when potassium is the principal electron source and neon is the carrier gas.

With film calibration curves, the uncorrected densitometer traces can be converted into plots of relative intensity vs wavelength. A typical pair of curves is that shown in Fig. 4. These are both from scans taken from the spectrum shown in Fig. 3(a), but at times 30 μsec apart, or more precisely, at positions on the film 3 mm apart. Note that although the intensity of the emission varies, the shape of the curve is constant. The thresholds near 8590, 8390, and 8275 Å are clearly evident, and there is some indication of a threshold in the vicinity of 8430 Å.

The tentative threshold measurements were collected from 18 microdensitometer tracings representing spectra of 11 different shocks. On five spectra, tracings corresponding to two different times were used and, in one instance, three different times were used. The time intervals chosen varied from 10 to 50 μsec. The various spectra were taken from shocks with K_2O_2 and with aluminum and cleansing-tissue supports, and with argon and neon carrier gas.

In any one spectrum, an intensity fluctuation was assigned as a threshold if its deviation from a smooth curve was equal to or greater than the height of the

intensity error bars of points within about a 25-Å neighborhood on either side or, in a few cases, if there were bands nearby, if the threshold (or band), were clearly distinguishable as such to the eye. For example, the upper curve of Fig. 3 was considered to exhibit thresholds at 8599, 8279, and a number of positions later assigned to K_2. It was not considered a useful spectrum for determining accurately the position of a threshold in the vicinity of 8390. (This particular curve, however, was considered evidence for the *existence* of a threshold in the 8350–8390-Å region.) In this spectrum, the 8390-Å threshold, if it is present, is simply too broad to be measured accurately. Such broadening was observed previously in intense absorption spectra of the halide ions.[5] On the other hand the lower tracing of Fig. 3, taken from a weaker spectrum than the upper tracing, is a fairly good example of the two higher-energy thresholds but was not considered to exhibit any lower-energy thresholds, even though it shows a drop in intensity in the 8600 region. In other words we have tried to be relatively conservative in assessing what constituted a threshold.

The results of the 18 observations can be seen conveniently in Fig. 5. We naturally attempted to assign all spectral features we could to known lines and bands. Essentially all the infrequently observed features were assigned. The K_2 bands[13,14] were the only prominent features, aside from atomic lines. Only the *three most frequently observed features were consistently unassignable as known spectra.* These features are the three thresholds we assign to Process (1).

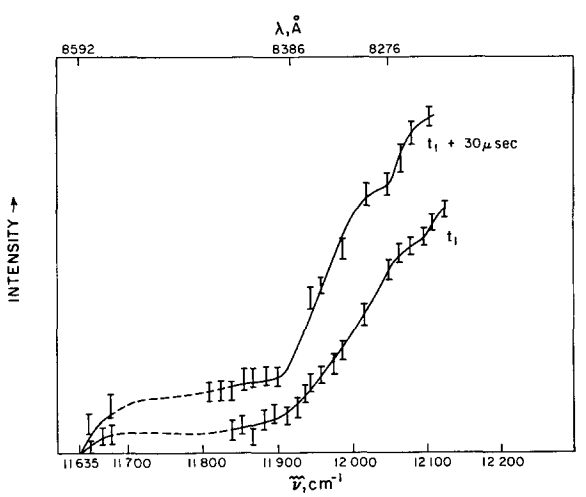

FIG. 4. Typical relative intensity curves for emission from radiative capture of electrons by oxygen atoms (K_2O_2 in Ne). Both curves were taken from the spectrum of Fig. 3 but correspond to times 30 μsec apart. The final wavelength determinations were made on the basis of 18 such curves. Intensity curves were all essentially flat from 8590 to the calcium line at 8662 and correspond to the base line of this figure. Beyond the calcium line, the film sensitivity drops rapidly with increasing wavelength.

[13] J. C. McLennan and D. S. Ainslie, Proc. Roy. Soc. (London) **A103**, 304 (1923).

[14] W. D. Crane and A. Christy, Phys. Rev. **36**, 421 (1930).

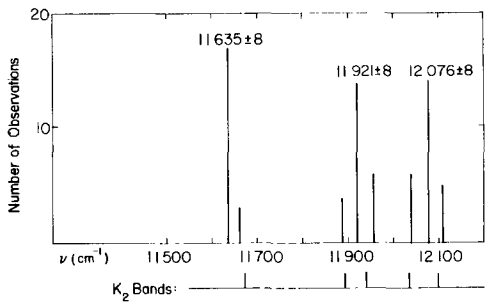

FIG. 5. Collected data from which threshold positions were measured. The position of each tentative threshold is indicated on the abscissa, and the number of times it was recorded, on the ordinate. A bandwidth of 15 cm^{-1} was chosen for the histogram construction. The rms deviations of the points contributing to the major peaks are 8 cm^{-1}. The more sparsely recorded features were essentially all assigned as K_2. The three most commonly recorded features are those assigned to Process (1). The dotted region on the abscissa between 11 700 and 11 800 cm^{-1} is the region obscured by calcium lines.

IV. RESULTS AND CONCLUSIONS

The conclusions drawn from the 18 microdensitometer tracings give the following wavelengths for the three clearly distinguished thresholds: 8592±6 Å, 8386±6 Å, and 8279±6 Å. The uncertainties are not independent; the separations between thresholds are only slightly more uncertain than any one threshold alone. There is also a possible threshold in the vicinity of 8429 Å, which is at best slightly above noise level. The relative intensities of the thresholds show considerable scatter, but those of Fig. 4 are typical; the 8386-Å threshold is two or three times as intense as the other two.

The separation of the two higher-energy thresholds is 155±12 cm^{-1}. We can identify this immediately with the separation of the well-known oxygen $^2P_2$–$^2P_1$ separation of 158 cm^{-1}.[15] This serves as an identification of the continuum, and is rather firmer than the purely circumstantial evidence of the variation of materials and conditions. These two transitions must both be to the $^2P_{\frac{3}{2}}$ state of O^-, since no higher-energy steps are observed.

The relative intensities of the various thresholds depend to a good approximation on the products of the statistical weights of initial and final states. This is because at such high temperatures, purely statistical population of the three J states of the neutral oxygen atom is attained. Therefore, the only other threshold of strength comparable to those at 8386 and 8276 Å is expected to lie at longer wavelengths, to be approximately as intense as the 8276-Å threshold, and to be separated from the most intense threshold by just the separation Δ, between O^-, $^2P_{\frac{1}{2}}$ and O^-, $^2P_{\frac{3}{2}}$. The separation we observe, between the 8592- and 8386-Å thresholds, is

$$\Delta = 285 \pm 15 \text{ cm}^{-1},$$

[15] C. E. Moore, Natl. Bur. Std. (U.S.) Circ. No. 467, 1 (1949).

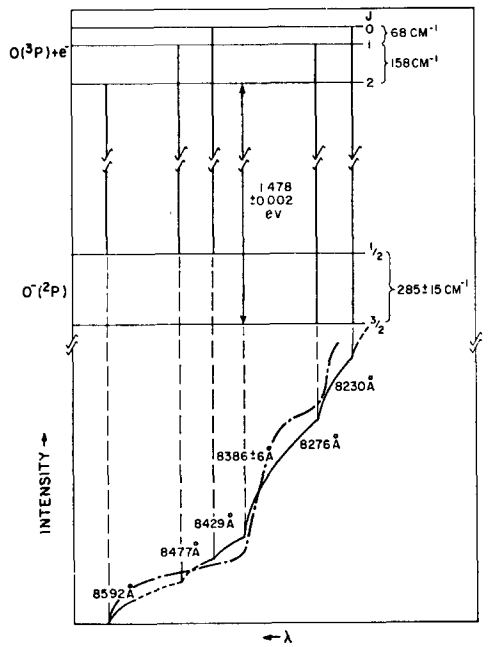

FIG. 6. Radiative capture of electrons by oxygen atoms. The upper part of the figure shows the three initial and two final states and all the transitions between them drawn to show their relative positions in a spectrum. The lower part of the figure, on the same wavelength (horizontal) scale, shows the shape of the total emission from Process (1); the wavelengths are taken from this work and, where necessary, from Ref. 13. The solid curve is based on theoretical intensities and experimental wavelengths, as measured in this work or as reported in Ref. 13. The solid curve is dotted in the region where there are interfering lines in the spectrum. The dash–dot curve is the upper curve from Fig. 4, exactly as drawn in that figure.

corresponding to a spin–orbit coupling constant of just two-thirds this value,

$$\lambda_0 = 190 \pm 10 \text{ cm}^{-1}.$$

The intensities of the observed thresholds at 8592 and 8276 are approximately the same.

The identification of the three thresholds is as shown in Fig. 6. The lowest-energy step at 8592 Å, corresponds to the transition $O^0(^3P_2)+e^- \rightarrow O^-(^2P_{\frac{1}{2}})$. The most intense step, at 8386 Å, corresponds to the electron-affinity transition, $O^0(^3P_2)+e^- \rightarrow O^-(^2P_{\frac{3}{2}})$. The emission starting at 8276 Å corresponds to $O^0(^3P_1)+e^- \rightarrow O^-(^2P_{\frac{3}{2}})$. The other three transitions can be predicted readily; $O^0(^3P_1)+e^- \rightarrow O^-(^2P_{\frac{1}{2}})$ is expected at 8477 Å, which is covered by lines of Ca^+; $O^0(^3P_0)+e \rightarrow O^-(^2P_{\frac{1}{2}})$ is predicted at 8429 Å, and is the weakest of the six thresholds; our possible weak transition occurs at just this wavelength. Finally the transition $O^0(^3P_0)+e^- \rightarrow O^-(^2P_{\frac{3}{2}})$ is expected at 8230 Å and is masked by the wing of the sodium line. The shape of the curve of Fig. 6 should be compared directly with the experimental curves of Fig. 4.

From the position of the strongest threshold, we calculate an electron affinity of the oxygen atom:

$$\text{E.A.(O)} = 1.478 \pm 0.002 \text{ eV}$$

or

$$34.10 \pm 0.04 \text{ kcal/mole}.$$

This value is slightly higher than the 1.465 eV obtained by crossed-beam measurements. However, the beam experiments required an assumption of the size of Δ to permit the determination of the affinity. The discrepancy between the two affinities, 0.013 eV, less the discrepancy between the extrapolated and observed Δ values, 0.006 eV, is just enough to bring the two measurements to the limits of the two estimates of uncertainty. The application of this correction is only approximate; nevertheless we feel justified in saying that the two methods are in essential agreement regarding the value of the electron affinity of the oxygen atom.

The spin–orbit coupling constant λ of a many-electron atom is unfortunately not just a function of $\langle r^{-3} \rangle$, even to a rough approximation. Blume and Watson have shown this clearly by calculating virtually all the contributions to λ from Hartree–Fock wavefunctions of a variety of atoms and positive ions.[16] Nevertheless in an isoelectric series, that part of λ which is truly an $\langle r^{-3} \rangle$ contribution takes values that are apparently proportional to the values of λ itself. We can use this observation to draw a crude and approximate inference about a size parameter for O^-. Specifically, we say

$$\langle r^{-3} \rangle_{O^-} \approx \langle r^{-3} \rangle_{F^0} [\Delta(O^-)/\Delta(F^0)].$$

From the calculations of Blume and Watson, we estimate the corresponding radius for fluorine $\langle r^{-3} \rangle_{F^0}^{-\frac{1}{3}} \approx 0.21$ Å; furthermore $\Delta(F^0) = 404$ cm^{-1} and $\Delta(O^-) = 285$ cm^{-1}, so that $\langle r^{-3} \rangle_{O^-}^{-\frac{1}{3}} \approx 0.24$ Å, or only about 15% larger than the corresponding value for the fluorine atom.

[16] M. Blume and R. E. Watson, Proc. Roy. Soc. (London) **A270**, 127 (1962); **A271**, 565 (1963).